

Optimization of RIS-aided SISO Systems Based on a Mutually Coupled Loaded Wire Dipole Model

Invited Paper

Nemanja Stefan Perović*, Le-Nam Tran[†], Marco Di Renzo*, and Mark F. Flanagan[†]

*Université Paris-Saclay, CNRS, CentraleSupélec, Laboratoire des Signaux et Systèmes
3 rue Joliot Curie, 91192, Gif-sur-Yvette, France

Email: nemanja-stefan.perovic@centralesupelec.fr, marco.di-renzo@universite-paris-saclay.fr.

[†]School of Electrical and Electronic Engineering, University College Dublin
Belfield, Dublin 4, D04 V1W8, Ireland

Email: nam.tran@ucd.ie, mark.flanagan@ieee.org.

Abstract—The electromagnetic (EM) features of reconfigurable intelligent surfaces (RISs) fundamentally determine their operating principles and performance. Motivated by these considerations, we study a single-input single-output (SISO) system in the presence of an RIS, which is characterized by a circuit-based EM-compliant model. Specifically, we model the RIS as a collection of thin wire dipoles controlled by tunable load impedances, and we propose a gradient-based algorithm for calculating the optimal impedances of the scattering elements of the RIS in the presence of mutual coupling. Furthermore, we prove the convergence of the proposed algorithm and derive its computational complexity in terms of number of complex multiplications. Numerical results show that the proposed algorithm provides better performance than a benchmark algorithm and that it converges in a shorter amount of time.

Index Terms—Reconfigurable intelligent surface (RIS), thin wire dipole model, mutual coupling, optimization.

I. INTRODUCTION

Reconfigurable intelligent surfaces (RISs) represent a new technology capable of shaping the radio wave propagation and thereby transform a generally unpredictable wireless channel into a controllable and programmable medium. An RIS is typically implemented as a thin metasurface that consists of low-cost and nearly passive radiating elements that can be electronically controlled to alter the wavefront of the impinging waves [1], [2]. By optimizing the reflection coefficients of the RIS elements, it is possible to overcome the adverse effects of uncontrolled wireless propagation, resulting in a variety of performance and implementation gains. The RIS technology can be used to improve the received power [3], achievable rate [4], [5], mutual information [6], [7], interference management [8] and coverage [9]. In the aforementioned papers, it is assumed that each RIS element can reflect any impinging radio wave with unitary power efficiency and an arbitrary phase shift, and that the electromagnetic (EM) coupling between adjacent RIS elements is negligible. However, these modeling assumptions generally overlook the EM characteristics and implementation aspects of RISs [10]. In order to obtain a more accurate prediction of the performance of RIS-aided communications, it is important to utilize RIS models that

take into account the EM properties of the RIS, and to develop efficient optimization algorithms based on these models.

In [11], the authors introduced a circuit-based model for the RIS elements, which explicitly accounts for the relationship between the amplitude and phase of the reflection coefficients. Using this model, they optimized the achievable rate. A transfer function for an RIS-aided communication system, where the RIS elements are modeled as thin wire dipoles driven by tunable impedances, was derived in [12]. This model accounts for the mutual coupling among the elements of the RIS, as well as the interactions between the transmitter, the receiver and the RIS, e.g., if they are in the near-field of each other. Building upon the model from [12], an algorithm to maximize the received signal power by optimizing the impedances of the RIS elements was proposed in [13]. The algorithm was developed for a single-input single-output (SISO) system, and the authors utilized an approximation for the transfer function that partially decouples the interactions between the transmitter, RIS, and receiver while accounting for the mutual coupling among co-located radiating elements. The algorithm introduced in [13] was generalized in [14] for optimizing the sum-rate of RIS-assisted multi-user multiple-input multiple-output (MIMO) channels by using the weighted minimum mean square error (MMSE) algorithm. More precisely, the algorithm introduced in [14] determines the optimal impedances of the RIS elements and the optimal precoding for each transmitter. Similarly, an MMSE-based algorithm that adjusts the transfer admittance matrix of an RIS in order to maximize the capacity of a point-to-point RIS-aided MIMO system was introduced in [15]. In [16], the authors proposed an EM-compliant RIS-aided communication model formulated in terms of scattering parameters. Based on the obtained circuit-based model, they optimized the scattering matrix of the RIS with the aim to maximize the received signal power.

Against this background, the contributions of this paper are as follows:

- We consider the circuit-based model introduced in [12] for an RIS-aided SISO system and aim to maximize the received signal power for the considered system.

- We introduce a gradient-based algorithm to find the optimal values of the tunable impedances of the RIS elements. Unlike the optimization algorithm in [13], which is based on an approximation of the transfer function with unknown impact on the final performance, the proposed algorithm relies on the exact formulation of the transfer function.
- We prove that the proposed algorithm is monotonically convergent and derive its computational complexity in terms of number of complex multiplications.
- We show through numerical simulations that the proposed algorithm provides similar or better performance than the best-known benchmark algorithm, while being significantly faster. Also, we demonstrate that reducing the inter-distance between adjacent RIS elements on a fixed-size RIS leads to improved performance, as long as the mutual coupling among the RIS elements is considered in the design.

Notation: Bold lower and upper case letters represent vectors and matrices, respectively. $(\cdot)^*$ denotes the complex conjugate operator. $\Re(\mathbf{x})$ and $\Im(\mathbf{x})$ denote the real and imaginary part operators of a vector \mathbf{x} , respectively. $\text{diag}(\mathbf{x})$ denotes a diagonal matrix whose diagonal entries are given by \mathbf{x} . For a matrix \mathbf{X} , $\text{vec}_d(\mathbf{X})$ denotes a vector whose elements are the diagonal elements of \mathbf{X} . \mathbf{X}^T and \mathbf{X}^\dagger denote the transpose and Hermitian transpose of \mathbf{X} , respectively. $\lambda_{\max}(\mathbf{X})$ denotes the largest singular value of \mathbf{X} . $\|\mathbf{X}\|$ denotes the Frobenius norm of \mathbf{X} and $|x|$ denotes the absolute value of x . $\nabla_{\mathbf{x}}f(\cdot)$ denotes the complex gradient of $f(\cdot)$ with respect to \mathbf{x} .

II. SYSTEM MODEL AND PROBLEM FORMULATION

A. System Model

We consider a communication system comprising of a single-antenna transmitter and receiver that communicate via an RIS. The RIS consists of N_{RIS} reflecting elements arranged in a rectangular formation and uniformly separated in both dimensions. For ease of representation, the transmit antenna, the receive antenna, and the reflecting elements of the RIS are modeled as thin wire dipoles made of perfectly conducting material. The dipole length, l , is assumed to be much larger than its radius, a , i.e., a thin wire approximation is assumed.

The transmitted signal is generated by a voltage source V_G with an internal impedance z_G , which is fed to the transmit dipole. At the reception, the receive dipole is connected to the load impedance z_L . The voltage at the port of the receiver is denoted by V_L . The EM interaction between the elements of the RIS is specified by the impedance matrix $\mathbf{Z}_{\text{SS}} \in \mathbb{C}^{N_{\text{RIS}} \times N_{\text{RIS}}}$, where $\mathbf{Z}_{\text{SS}}(q, p)$ characterizes the mutual coupling induced by the p -th element on the q -th element. The elements (thin wire dipoles) of the RIS are connected to tunable impedances, denoted by the vector $\mathbf{z}_{\text{RIS}} \in \mathbb{C}^{N_{\text{RIS}} \times 1}$. More precisely, the s -th element of \mathbf{z}_{RIS} represents the tunable impedance connected to the s -th RIS element. We assume that the tunable impedances \mathbf{z}_{RIS} have a fixed real part (i.e., the resistance is fixed), which satisfies the condition

$\mathbf{z}_{\text{RIS,Re}}(s) = R_0 \geq 0$ for $s = 1, \dots, N_{\text{RIS}}$, where $\mathbf{z}_{\text{RIS,Re}} \triangleq \Re(\mathbf{z}_{\text{RIS}})$, since the RIS is a nearly-passive device and R_0 accounts for the internal losses of the tuning circuits. On the other hand, the imaginary part of each element of \mathbf{z}_{RIS} , i.e., $\mathbf{z}_{\text{RIS,Im}} \triangleq \Im(\mathbf{z}_{\text{RIS}})$, is an arbitrary real number, whose set of feasible values is $[z_{\min}, z_{\max}]^1$, which is to be determined by the proposed optimization algorithm. For ease of notation, we define the equivalent RIS impedance matrix as follows:

$$\mathbf{Z}_{\text{SE}} = \mathbf{Z}_{\text{SS}} + \text{diag}(\mathbf{z}_{\text{RIS}}) \in \mathbb{C}^{N_{\text{RIS}} \times N_{\text{RIS}}}. \quad (1)$$

It was shown in [12] that the end-to-end transfer function (i.e., the equivalent communication channel) is given by

$$h_{\text{E2E}} = \frac{V_L}{V_G} = \frac{z_L \phi_{\text{TR}}}{\tilde{z}_T \tilde{z}_R - \phi_{\text{TR}}^2} \quad (2)$$

where $\tilde{z}_T = z_G + \phi_{\text{TT}}$ and $\tilde{z}_R = z_L + \phi_{\text{RR}}$, and the notation

$$\phi_{\text{KL}} = z_{\text{KL}} - \mathbf{z}_{\text{KS}} \mathbf{Z}_{\text{SE}}^{-1} \mathbf{z}_{\text{SL}} \quad (3)$$

for $K, L \in \{\text{T}, \text{R}\}$ is utilized. Specifically, z_{TT} (respectively, z_{RR}) represents the self impedance of the transmit antenna (respectively, receive antenna), while $z_{\text{TR}} = z_{\text{RT}}$ denotes the mutual impedance between the transmit and receive antennas. The vector $\mathbf{z}_{\text{KS}} \in \mathbb{C}^{1 \times N_{\text{RIS}}}$ contains the mutual impedances between the transmit antenna and the RIS elements if $K = \text{T}$ or between the receive antenna and the RIS elements if $K = \text{R}$; and $\mathbf{z}_{\text{SL}} \in \mathbb{C}^{N_{\text{RIS}} \times 1}$ denotes the vector containing the mutual impedances between the RIS elements and the transmit antenna if $L = \text{T}$ or between the RIS elements and the receive antenna if $L = \text{R}$ ².

B. Problem Formulation

In a SISO system, the most important performance metrics, such as the channel capacity and the bit error rate (BER), are primarily determined by the signal power at the receive antenna. Therefore, our primary objective is to maximize this power by finding the optimal values for the tunable impedances at the RIS.

Formally written, the optimization problem is given by

$$\underset{\mathbf{z}_{\text{RIS}}}{\text{maximize}} f(\mathbf{z}_{\text{RIS}}) = |h_{\text{E2E}}|^2 = \left| \frac{z_L \phi_{\text{TR}}}{\tilde{z}_T \tilde{z}_R - \phi_{\text{TR}}^2} \right|^2 \quad (4a)$$

$$\text{subject to } \mathbf{z}_{\text{RIS,Re}}(s) = R_0, \forall s \quad (4b)$$

$$\mathbf{z}_{\text{RIS,Im}}(s) \in [z_{\min}, z_{\max}], \forall s. \quad (4c)$$

III. PROPOSED OPTIMIZATION ALGORITHM

To solve the optimization problem in (4), we propose an efficient gradient-based method, which iteratively adjusts the imaginary parts of \mathbf{z}_{RIS} (i.e., $\mathbf{z}_{\text{RIS,Im}}$). It is worth noting that this method can be generalized to simultaneously optimize the real and the imaginary parts of \mathbf{z}_{RIS} ³.

¹This feasible set is chosen to account for all possible imaginary parts of \mathbf{z}_{RIS} that can be realized by utilizing existing tunable components.

²It is worth noting that the mutual impedances depend on the system geometry, i.e., the relative position and orientation of the transmitter, receiver and RIS, which are assumed to be fixed in this work. Also, finding the optimal position and orientation of the RIS in this context is an interesting open issue.

³The optimization of $\mathbf{z}_{\text{RIS,Re}}$ implies that the RIS may also consist of active reflecting elements. In this case, the RIS would no longer be a nearly-passive device and for this reason we focus solely on optimizing $\mathbf{z}_{\text{RIS,Im}}$. The RIS may, however, be still a globally-passive device, as elaborated in [10].

Before presenting the actual optimization algorithm for \mathbf{z}_{RIS} , we provide the gradient of $f(\mathbf{z}_{\text{RIS}})$ with respect to $\mathbf{z}_{\text{RIS,Im}}$.

Lemma 1. *The gradient of $f(\mathbf{z}_{\text{RIS}})$ with respect to $\mathbf{z}_{\text{RIS,Im}}$ is given by*

$$\nabla_{\mathbf{z}_{\text{RIS,Im}}} f(\mathbf{z}_{\text{RIS}}) = 2\mathcal{J}(h_{\text{E2E}} \text{vec}_d(\mathbf{E}^*)), \quad (5)$$

where

$$\mathbf{E} = z_{\text{L}} \mathbf{A} \mathbf{Z}_{\text{SE}}^{-1} ((2a\phi_{\text{TR}}^2 + 1) \mathbf{z}_{\text{SR}} \mathbf{z}_{\text{TS}} - a\phi_{\text{TR}} \tilde{\mathbf{z}}_{\text{R}} \mathbf{z}_{\text{ST}} \mathbf{z}_{\text{TS}} - a\phi_{\text{TR}} \tilde{\mathbf{z}}_{\text{T}} \mathbf{z}_{\text{SR}} \mathbf{z}_{\text{RS}}) \mathbf{Z}_{\text{SE}}^{-1} \quad (6)$$

and $a = (\tilde{\mathbf{z}}_{\text{T}} \tilde{\mathbf{z}}_{\text{R}} - \phi_{\text{TR}}^2)^{-1}$.

Proof: See Appendix A. \blacksquare

Given the gradient in Lemma 1, the proposed optimization algorithm is based on a line search procedure as detailed in Algorithm 1. Specifically, the elements of $\mathbf{z}_{\text{RIS}}^{(n+1)}$ at the $(n+1)$ -th iteration of the algorithm are obtained as follows. First, we update the values of the impedances of the RIS elements based on $\mathbf{z}_{\text{RIS}}^{(n+1)} = R_0 + jP_Z(\mathbf{z}_{\text{RIS,Im}}^{(n)} + \mu_n \nabla_{\mathbf{z}_{\text{RIS,Im}}} f(\mathbf{z}_{\text{RIS}}^{(n)}))$, where the impedance projection $\tilde{\mathbf{z}}_{\text{RIS,Im}} = P_Z(\mathbf{z}_{\text{RIS,Im}})$ is given by

$$\tilde{\mathbf{z}}_{\text{RIS,Im}}(s) = \begin{cases} z_{\text{max}} & \mathbf{z}_{\text{RIS,Im}}(s) > z_{\text{max}} \\ z_{\text{min}} & \mathbf{z}_{\text{RIS,Im}}(s) < z_{\text{min}} \\ \mathbf{z}_{\text{RIS,Im}}(s) & \text{otherwise} \end{cases} \quad (7)$$

for $s \in \{1, 2, \dots, N_{\text{RIS}}\}$. Then, we assume that the gradient step size μ_n is updated based on a line search procedure. Also, we utilize the following quadratic approximation for the function $f(\mathbf{z}_{\text{RIS}})$ around $\mathbf{z}_{\text{RIS}}^{(n)}$:

$$Q_{\mu_n}(\mathbf{z}_{\text{RIS}}; \mathbf{z}_{\text{RIS}}^{(n)}) = f(\mathbf{z}_{\text{RIS}}^{(n)}) + \langle \nabla_{\mathbf{z}_{\text{RIS,Im}}} f(\mathbf{z}_{\text{RIS}}^{(n)}), \mathbf{z}_{\text{RIS,Im}} - \mathbf{z}_{\text{RIS,Im}}^{(n)} \rangle - \frac{1}{2\mu_n} \|\mathbf{z}_{\text{RIS,Im}} - \mathbf{z}_{\text{RIS,Im}}^{(n)}\|^2 \quad (8)$$

where $\langle \mathbf{x}, \mathbf{y} \rangle = \mathbf{x}^T \mathbf{y}$. If $Q_{\mu_n}(\mathbf{z}_{\text{RIS}}^{(n+1)}; \mathbf{z}_{\text{RIS}}^{(n)}) > f(\mathbf{z}_{\text{RIS}}^{(n+1)})$ (i.e., a lower bound is not achieved yet), we keep decreasing the step size μ_n until a quadratic minorant is achieved. It is worth noting that the proposed procedure terminates after a finite number of steps, since $f(\mathbf{z}_{\text{RIS}}^{(n+1)})$ is Lipschitz continuous [17]. To speed up the convergence of Algorithm 1, the step size is readjusted to the initial value after every 1000 iterations.

IV. CONVERGENCE AND COMPLEXITY ANALYSIS

A. Convergence Analysis

In this subsection, we analyze the convergence of the proposed algorithm. Let $L_{\mathbf{z}_{\text{RIS,Im}}}$ be the Lipschitz constant of $\nabla_{\mathbf{z}_{\text{RIS,Im}}} f(\mathbf{z}_{\text{RIS}})$. Then

$$f(\mathbf{z}_{\text{RIS}}^{(n+1)}) \geq f(\mathbf{z}_{\text{RIS}}^{(n)}) + \langle \nabla_{\mathbf{z}_{\text{RIS,Im}}} f(\mathbf{z}_{\text{RIS}}^{(n)}), \mathbf{z}_{\text{RIS,Im}}^{(n+1)} - \mathbf{z}_{\text{RIS,Im}}^{(n)} \rangle - \frac{L_{\mathbf{z}_{\text{RIS,Im}}}}{2} \|\mathbf{z}_{\text{RIS,Im}}^{(n+1)} - \mathbf{z}_{\text{RIS,Im}}^{(n)}\|^2. \quad (9)$$

Since the line search procedure ensures $Q_{\mu_n}(\mathbf{z}_{\text{RIS}}^{(n+1)}; \mathbf{z}_{\text{RIS}}^{(n)}) \leq f(\mathbf{z}_{\text{RIS}}^{(n+1)})$, we have

$$\langle \nabla_{\mathbf{z}_{\text{RIS,Im}}} f(\mathbf{z}_{\text{RIS}}^{(n)}), \mathbf{z}_{\text{RIS,Im}}^{(n+1)} - \mathbf{z}_{\text{RIS,Im}}^{(n)} \rangle - \frac{1}{2\mu_n} \|\mathbf{z}_{\text{RIS,Im}}^{(n+1)} - \mathbf{z}_{\text{RIS,Im}}^{(n)}\|^2 \geq 0 \quad (10)$$

Algorithm 1: Proposed optimization algorithm

Input: $\mathbf{z}_{\text{RIS}}^{(0)}, \mu_{\text{init}}$
1 Set $n \leftarrow 0$
2 Set $\mu_0 \leftarrow \mu_{\text{init}}$
3 **repeat**
4 **repeat**
5 Set $\mathbf{z}_{\text{RIS}}^{(n+1)} = R_0 + jP_Z(\mathbf{z}_{\text{RIS,Im}}^{(n)} + \mu_n \nabla_{\mathbf{z}_{\text{RIS,Im}}} f(\mathbf{z}_{\text{RIS}}^{(n)}))$
6 **if** $f(\mathbf{z}_{\text{RIS}}^{(n+1)}) < Q_{\mu_n}(\mathbf{z}_{\text{RIS}}^{(n+1)}; \mathbf{z}_{\text{RIS}}^{(n)})$ **then**
7 $\mu_n \leftarrow \kappa \mu_n$ /* $0 < \kappa < 1$ */
8 **end**
9 **until** $f(\mathbf{z}_{\text{RIS}}^{(n+1)}) \geq Q_{\mu_n}(\mathbf{z}_{\text{RIS}}^{(n+1)}; \mathbf{z}_{\text{RIS}}^{(n)})$
10 $n \leftarrow n + 1$
11 **if** $\text{mod}(n, 1000) = 0$ **then**
12 $\mu_n \leftarrow \mu_{\text{init}}$
13 **end**
14 **until** a stopping criterion is met

Combining (9) and (10), we obtain

$$f(\mathbf{z}_{\text{RIS}}^{(n+1)}) \geq f(\mathbf{z}_{\text{RIS}}^{(n)}) + \left[\frac{1}{2\mu_n} - \frac{L_{\mathbf{z}_{\text{RIS,Im}}}}{2} \right] \|\mathbf{z}_{\text{RIS,Im}}^{(n+1)} - \mathbf{z}_{\text{RIS,Im}}^{(n)}\|^2. \quad (11)$$

If $\mu_n < 1/L_{\mathbf{z}_{\text{RIS,Im}}}$, we have $f(\mathbf{z}_{\text{RIS}}^{(n+1)}) > f(\mathbf{z}_{\text{RIS}}^{(n)})$ and hence the objective function is monotonically increasing. Also, we note that the considered feasible set is a compact set. Furthermore, the objective function $f(\mathbf{z}_{\text{RIS}})$ can be proved to be a continuous function. Due to space limitations, we provide only a short sketch for the proof of the continuity of $f(\mathbf{z}_{\text{RIS}})$. From the definition of ϕ_{TR}

$$\phi_{\text{TR}} = z_{\text{TR}} - \mathbf{z}_{\text{TS}} \mathbf{Z}_{\text{SE}}^{-1} \mathbf{z}_{\text{SR}} \quad (12)$$

we have

$$|\phi_{\text{TR}}| \leq |z_{\text{TR}}| + |\mathbf{z}_{\text{TS}} \mathbf{Z}_{\text{SE}}^{-1} \mathbf{z}_{\text{SR}}| \quad (13)$$

$$\leq \lambda_{\text{max}}(\mathbf{Z}_{\text{SE}}^{-1}) \|\mathbf{z}_{\text{TS}}\| \|\mathbf{z}_{\text{SR}}\|. \quad (14)$$

Since $\mathbf{Z}_{\text{SE}} = \mathbf{Z}_{\text{SS}} + \text{diag}(\mathbf{z}_{\text{RIS}}) \succeq \text{diag}(\mathbf{z}_{\text{RIS}})$, we obtain $\lambda_{\text{max}}(\mathbf{Z}_{\text{SE}}^{-1}) \leq \frac{1}{R_0}$, which results in

$$|\phi_{\text{TR}}| \leq \frac{1}{R_0} \|\mathbf{z}_{\text{TS}}\| \|\mathbf{z}_{\text{SR}}\| \quad (15)$$

Next we need to prove that the term $\tilde{\mathbf{z}}_{\text{T}} \tilde{\mathbf{z}}_{\text{R}} - \phi_{\text{TR}}^2$ can not be equal to zero. Since the transmit and receive antenna are usually far from each other, it typically holds that $|z_{\text{TT}}| \gg |z_{\text{TR}}|$ and $|z_{\text{RR}}| \gg |z_{\text{TR}}|$. Thus, the term z_{TR} can be ignored for the analysis of the continuity of $f(\mathbf{z}_{\text{RIS}})$.

Finally, we conclude that $f(\mathbf{z}_{\text{RIS}}^{(n)})$ is bounded from above due to the continuity of $f(\mathbf{z}_{\text{RIS}})$ and the compactness of the feasible set. Therefore, the objective sequence $\{f(\mathbf{z}_{\text{RIS}}^{(n)})\}$ is provably convergent.

B. Complexity Analysis

In this subsection, the computational complexity of the proposed algorithm is evaluated in terms of number of complex multiplications. The inversion of the matrix \mathbf{Z}_{SE} requires $\mathcal{O}(N_{\text{RIS}}^3)$ multiplications. Additional $\mathcal{O}(N_{\text{RIS}}^2)$ multiplications are needed to calculate ϕ_{KL} for $K, L \in \{\text{T}, \text{R}\}$ in (3). Also, we observe that the complexity of each term

in brackets in (6) is $\mathcal{O}(N_{\text{RIS}}^2)$, and multiplying the central term in brackets with $\mathbf{Z}_{\text{SE}}^{-1}$ on the left-hand and right-hand sides requires $\mathcal{O}(2N_{\text{RIS}}^3)$ multiplications. Also, the multiplication with $z_{\text{L}}a$ has a complexity of $\mathcal{O}(N_{\text{RIS}}^2)$. Hence, the total complexity of calculating the gradient $\nabla_{\mathbf{z}_{\text{RIS,Im}}} f(\mathbf{z}_{\text{RIS}})$ is approximately $\mathcal{O}(3N_{\text{RIS}}^3)$. In the inner loop of Algorithm 1 (Steps 4-9), $\mathcal{O}(N_{\text{RIS}}^3 + N_{\text{RIS}}^2)$ multiplications are needed to calculate $f(\bar{\mathbf{z}}_{\text{RIS}}^{(n+1)})$. The additional complexity of computing $Q_{\mu_n}(\bar{\mathbf{z}}_{\text{RIS}}^{(n+1)}; \bar{\mathbf{z}}_{\text{RIS}}^{(n)})$ can be neglected. Hence, the complexity per iteration of the proposed algorithm (i.e., computing $\bar{\mathbf{z}}_{\text{RIS}}^{(n+1)}$ from $\bar{\mathbf{z}}_{\text{RIS}}^{(n)}$) is $\mathcal{O}(3N_{\text{RIS}}^3 + L_P(N_{\text{RIS}}^3 + N_{\text{RIS}}^2))$, where L_P is the average number of inner loops for the line search procedure. The value of L_P can be estimated by performing numerical simulations based on the proposed method. The (average) total complexity of the proposed method is given by

$$C_P = \mathcal{O}(I_P(3N_{\text{RIS}}^3 + L_P(N_{\text{RIS}}^3 + N_{\text{RIS}}^2))), \quad (16)$$

where I_P is the average number of iterations of the proposed method.

V. SIMULATION RESULTS

In this section, we present numerical results to demonstrate the performance of the proposed optimization method. As a benchmark, we consider the optimization algorithm introduced in [13], which also optimizes the signal power at the receive antenna, but uses the following approximated end-to-end transfer function

$$h_{\text{E2E}} \approx h_{\text{E2E,APP}} = \mathcal{Y}_0(z_{\text{RT}} - \mathbf{z}_{\text{RS}}\mathbf{Z}_{\text{SE}}^{-1}\mathbf{z}_{\text{ST}}) = \mathcal{Y}_0\phi_{\text{RT}} \quad (17)$$

where $\mathcal{Y}_0 = z_{\text{L}}(z_{\text{L}} + z_{\text{RR}})^{-1}(z_{\text{G}} + z_{\text{TT}})^{-1}$. In each iteration, the benchmark algorithm updates the RIS impedances as $\mathbf{z}_{\text{RIS}}^{(n+1)} = \mathbf{z}_{\text{RIS}}^{(n)} + j\delta \sin(\theta)$, where $\delta = \Re(\mathbf{Z}_{\text{SS}}(1, 1))/M$ and θ is calculated according to [13, Eq. (24)]. First, we present the obtained objective values for the proposed and benchmark algorithms. Next, we compare the computational complexities and the execution times of the two algorithms. Finally, we analyze the trade-off between the inter-distance among the RIS elements and the number of RIS elements.

The simulation setup considered in this study assumes a frequency equal to $f = 3.5$ GHz, whose corresponding wavelength is $\lambda = 8.57$ cm. The positions of the transmit antenna, receive antenna, and the elements of the RIS are specified by Cartesian coordinates. The RIS has a square shape and is placed on the yz -plane with its center located in $(0, 0, 0)$. The positions of the transmit and the receive antennas are $(10 \text{ m}, -1 \text{ m}, 0 \text{ m})$ and $(10 \text{ m}, 99 \text{ m}, 0 \text{ m})$, respectively, resulting in a distance of 100 m. The number of RIS elements is $N_{\text{RIS}} = 14 \times 14 = 196$. The inter-distance between the RIS elements in both dimensions is $\lambda/4$, and the RIS size is approximately 30×30 cm. According to Section II, the transmit and receive antennas, and the reflecting elements of the RIS are modeled as thin wire dipoles with radius $a = \lambda/500$ and length $l = \lambda/32$, and they are assumed to be placed parallel to the z -axis. Also, we assume $z_{\text{G}} = z_{\text{L}} = (50 + 50j)$ Ohm. The initial value for the step size in Algorithm 1 is $\mu_{\text{init}} = 10^{25}$ and $\kappa = 1/2$. The allowed maximum and minimum values for $\mathbf{z}_{\text{RIS,Im}}$ are $z_{\text{max}} = -z_{\text{min}} = 10^4$ Ohm, respectively. For the

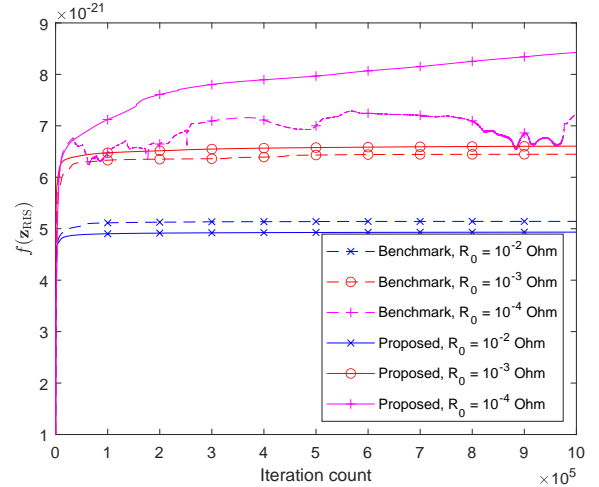


Fig. 1. Objective functions of the proposed and benchmark algorithms versus the number of iterations.

benchmark algorithm, \mathbf{z}_{RIS} is initialized using the optimal \mathbf{z}_{RIS} for the case of no mutual coupling between the RIS elements [13, Eq. (10)] and $M = 50$. For the proposed algorithm, the numerical experiments have shown that the best results are obtained if \mathbf{z}_{RIS} is initialized as $\mathbf{z}_{\text{RIS}}^{(0)} = R_0 - j\Im(\text{vec}_d(\mathbf{Z}_{\text{SS}}))$. Additionally, it is assumed that the direct link is very weak, allowing us to ignore it, i.e., $z_{\text{TR}} = z_{\text{RT}} = 0$. All impedances are calculated from [12]. The algorithms are developed using MATLAB R2022a and are run on a computer with a processor frequency of 2.8 GHz.

Fig. 1 plots the objective functions of the proposed and benchmark algorithms against the number of iterations. The proposed algorithm shows a performance advantage compared to the benchmark algorithm if the real part of \mathbf{z}_{RIS} is smaller than or equal to 10^{-3} Ohm. Moreover, when the real part of \mathbf{z}_{RIS} is very small (i.e., 10^{-4} Ohm), the benchmark algorithm is not monotonically convergent. This can be explained by the following argument. When the real part of \mathbf{z}_{RIS} is very small, the algorithm tends to update the imaginary part of \mathbf{z}_{RIS} so that \mathbf{Z}_{SE} becomes almost singular. On the other hand, the impedance increment in an iteration of the benchmark algorithm in [13] has to satisfy the condition $\delta \ll 1/\|\mathbf{Z}_{\text{SE}}^{-1}\|$, which is hard to achieve when \mathbf{Z}_{SE} tends to be singular and thus the algorithm is not convergent. The convergence of the benchmark algorithm can, however, be improved by setting a very small value of δ , but the corresponding convergence time significantly increases in this case. The results shown in Fig. 1 are obtained by setting $\delta = 0.0039$. In [18], the authors tackled this issue by adding the condition on δ as a constraint of the formulated optimization problem.

In Fig. 2, we compare the objective values of the proposed and benchmark algorithms versus the execution time using the same simulation setup as in Fig. 1. When both algorithms are monotonically convergent, the proposed algorithm clearly requires less time to converge. As both algorithms optimize all the RIS tunable impedances in one iteration, the proposed gradient-based optimization turns out to be more time efficient

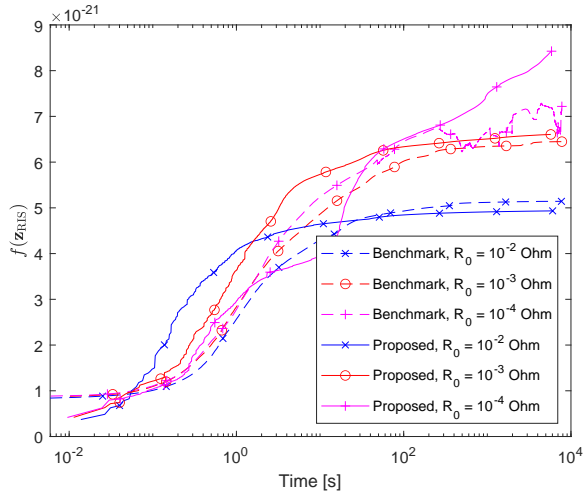


Fig. 2. Objective functions of the proposed and benchmark algorithms versus the execution time.

TABLE I

COMPARISON OF THE COMPUTATIONAL COMPLEXITY REQUIRED BY THE PROPOSED ALGORITHM (C_P) AND BENCHMARK ALGORITHM (C_B) TO ACHIEVE 95% OF THE OBJECTIVE VALUES AT THE 10^6 -TH ITERATION.

R_0 [Ohm]	L_P	I_P	C_P	I_B	C_B
10^{-2}	6	3208	1.94×10^{11}	9683	7.32×10^{10}
10^{-3}	6	10935	6.61×10^{11}	22138	1.68×10^{11}

than the benchmark algorithm.

The computational complexity required by the proposed and benchmark algorithms to reach 95% of the objective values at the 10^6 -th iteration is presented⁴ in Table I. The computational complexity of the benchmark algorithm is $C_B = \mathcal{O}(I_B(N_{\text{RIS}}^3 + N_{\text{RIS}}^2))$, where I_B is the number of iterations to reach convergence. The proposed algorithm needs fewer iterations to achieve the target value of the objective function compared to the benchmark algorithm. However, due to multiple inner loops in the line search procedure, the proposed algorithm has a higher computational complexity compared to the benchmark algorithm. In general, we conclude that the proposed algorithm has a higher computational complexity, but the execution time is shorter.

To analyze the execution time in more detail, Table II presents the time required by the proposed algorithm (T_P) and benchmark algorithm (T_B) to achieve 95% of the objective values at the 10^6 -th iteration. The results indicate that the proposed algorithm generally requires considerably less time to achieve the target objective function value.

In Fig. 3, we show the objective values of the proposed algorithm as a function of the inter-distance between adjacent RIS elements while keeping the size of the RIS fixed. As a result, the number of RIS elements varies with the inter-distance between the RIS elements. For an RIS whose size is 15×15 cm and the inter-distance is $\lambda/2$, $\lambda/4$ and $\lambda/8$, the number of RIS elements is 16, 49, and 196, respectively. The real part of each element of \mathbf{z}_{RIS} is $R_0 = 10^{-3}$ Ohm.

⁴We do not present the computational complexity for $R_0 = 10^{-4}$ Ohm, since the benchmark algorithm is not monotonically convergent for the considered value of δ , and it is difficult to determine the computation time.

TABLE II

TIME REQUIRED BY THE PROPOSED ALGORITHM (T_P) AND BENCHMARK ALGORITHM (T_B) TO ACHIEVE 95% OF THE OBJECTIVE VALUES AT THE 10^6 -TH ITERATION.

R_0 [Ohm]	T_P [ms]	T_B [ms]
10^{-2}	16	67
10^{-3}	62	173

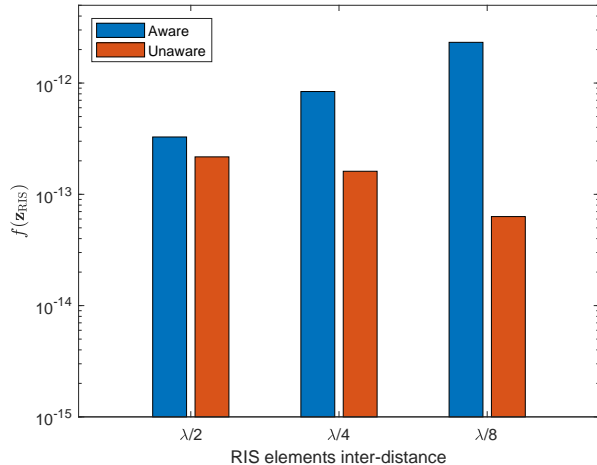


Fig. 3. Objective function of the proposed algorithm versus the inter-distance between adjacent RIS elements for an RIS of fixed size ($R_0 = 10^{-3}$ Ohm).

Also, we assume that the lengths of the transmit and receive antenna dipoles are $\lambda/2$. Simulation results are generated for the mutual coupling aware and the mutual coupling unaware cases⁵. Similar to [13, Fig. 3] and [14], the objective function monotonically increases with the number of RIS elements in the mutual coupling aware case, while it monotonically decreases in the mutual coupling unaware case. This behavior implies that taking the mutual coupling into account at the design stage can enhance the system performance⁶. Also, the larger values of the objective function with respect to Fig. 1 are attributed to the larger size of the transmit and receive antenna dipoles.

Fig. 4 reports results from a setup analogous to that of Fig. 3, with the exception that the length of the RIS (dipole) elements is equal to the inter-distance between them. In the mutual coupling aware case, the objective function is slightly larger than Fig. 3. When the mutual coupling is disregarded, on the other hand, the objective function has a significantly lower value. This is attributed to the more profound impact of the mutual coupling, due to the increased size of the RIS elements, if it is not taken into account by design.

⁵In the mutual coupling aware case, the proposed algorithm takes the mutual coupling between the RIS elements into account at the optimization stage (i.e., by design). On the other hand, the mutual coupling is not considered (i.e., ignored) by the proposed algorithm in the mutual coupling unaware case.

⁶These results are obtained under the assumption that the number of RIS elements increases as the inter-distance decreases, i.e., the impact of the mutual coupling become more noticeable. This is different from the results reported in [13, Fig. 2], where the inter-distances decreases but the number of RIS element is kept fixed. In [13, Fig. 2], we see a slight decrease of the objective function as the inter-distance decreases, even in the mutual coupling aware case.

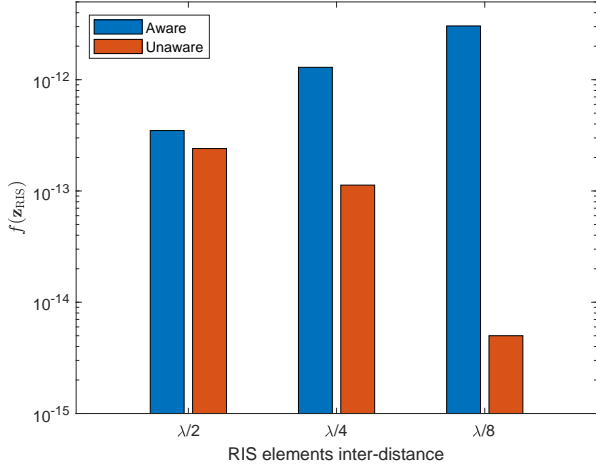


Fig. 4. Objective function of the proposed algorithm versus the inter-distance between adjacent RIS elements for an RIS of fixed size and for a variable length of the RIS elements ($R_0 = 10^{-3}$ Ohm).

VI. CONCLUSION

In this paper, we considered a mutually coupled loaded wire dipole model for RIS-aided communications and proposed a gradient-based algorithm for optimizing the impedances of the RIS elements. We proved that the proposed algorithm is monotonically convergent and derived its computational complexity. Our numerical results showed that the proposed algorithm achieves better performance compared to a recent benchmark algorithm and, at the same time, requires significantly less time to converge. Also, we demonstrated that reducing the inter-distance between adjacent RIS elements, by keeping the size of the RIS fixed, positively impacts the system performance, provided that the mutual coupling is incorporated into the design during the optimization stage.

APPENDIX A

PROOF OF LEMMA 1

Differentiating the objective function, we have

$$df(\mathbf{z}_{\text{RIS}}) = d|h_{\text{E2E}}|^2 = h_{\text{E2E}}^* dh_{\text{E2E}} + h_{\text{E2E}} dh_{\text{E2E}}^* \quad (18)$$

After differentiating the transfer function h_{E2E} and performing some simple algebraic manipulations, we obtain

$$dh_{\text{E2E}} = z_L a \left((2a\phi_{\text{TR}}^2 + 1) d\phi_{\text{TR}} - a\phi_{\text{TR}} \tilde{z}_R d\tilde{z}_T - a\phi_{\text{TR}} \tilde{z}_T d\tilde{z}_R \right) \quad (19)$$

where we use the following identity $d\phi_{\text{KL}} = \mathbf{z}_{\text{KS}} \mathbf{Z}_{\text{SE}}^{-1} d(\text{diag}(\mathbf{z}_{\text{RIS}})) \mathbf{Z}_{\text{SE}}^{-1} \mathbf{z}_{\text{SL}}$ for $K, L \in \{\text{T}, \text{R}\}$.

Considering the definition of \mathbf{E} in (6), we can write

$$dh_{\text{E2E}} = \text{Tr}(\mathbf{E} d\mathbf{z}_{\text{RIS}}) = (\text{vec}_d(\mathbf{E}))^\top d\mathbf{z}_{\text{RIS}} \quad (20)$$

and thus

$$df(\mathbf{z}_{\text{RIS}}) = h_{\text{E2E}}^* (\text{vec}_d(\mathbf{E}))^\top d\mathbf{z}_{\text{RIS}} + h_{\text{E2E}} (\text{vec}_d(\mathbf{E}^*))^\top d\mathbf{z}_{\text{RIS}}^* \quad (21)$$

Substituting $d\mathbf{z}_{\text{RIS}} = j d\mathbf{z}_{\text{RIS}, \text{Im}}$ into the previous expression, we obtain

$$df(\mathbf{z}_{\text{RIS}}) = 2\mathcal{J}(h_{\text{E2E}} (\text{vec}_d(\mathbf{E}^*))^\top) d\mathbf{z}_{\text{RIS}, \text{Im}} \quad (21)$$

Finally, we have

$$\nabla_{\mathbf{z}_{\text{RIS}, \text{Im}}} f(\mathbf{z}_{\text{RIS}}) = 2\mathcal{J}(h_{\text{E2E}} \text{vec}_d(\mathbf{E}^*)) \quad (22)$$

which completes the proof.

ACKNOWLEDGMENT

This work was supported in part by the European Commission through the H2020 SURFER project (agreement number 101030536), the H2020 ARIADNE project (agreement number 871464), the H2020 RISE-6G project (agreement number 101017011), and by the Agence Nationale de la Recherche (ANR) through the ANR PEPR-5G project.

REFERENCES

- [1] M. Di Renzo *et al.*, "Smart radio environments empowered by reconfigurable intelligent surfaces: How it works, state of research, and road ahead," *IEEE J. Sel. Areas Commun.*, vol. 38, no. 11, pp. 2450–2525, Nov. 2020.
- [2] C. Pan *et al.*, "An overview of signal processing techniques for RIS/IRS-aided wireless systems," *IEEE J. Sel. Top. Signal Process.*, vol. 16, no. 5, pp. 883–917, Aug. 2022.
- [3] X. Qian *et al.*, "Beamforming through reconfigurable intelligent surfaces in single-user MIMO systems: SNR distribution and scaling laws in the presence of channel fading and phase noise," *IEEE Wireless Commun. Lett.*, vol. 10, no. 1, pp. 77–81, Jan. 2021.
- [4] N. S. Perović *et al.*, "Achievable rate optimization for MIMO systems with reconfigurable intelligent surfaces," *IEEE Trans. Wireless Commun.*, vol. 20, no. 6, pp. 3865–3882, Jun. 2021.
- [5] Q. Wu and R. Zhang, "Intelligent reflecting surface enhanced wireless network via joint active and passive beamforming," *IEEE Trans. Wireless Commun.*, vol. 18, no. 11, pp. 5394–5409, Nov. 2019.
- [6] N. S. Perović *et al.*, "Optimization of RIS-aided MIMO systems via the cutoff rate," *IEEE Wireless Commun. Lett.*, vol. 10, no. 8, pp. 1692–1696, Aug. 2021.
- [7] R. Karasik *et al.*, "Adaptive coding and channel shaping through reconfigurable intelligent surfaces: An information-theoretic analysis," *IEEE Trans. Commun.*, vol. 69, no. 11, pp. 7320–7334, Nov. 2021.
- [8] M. Fu *et al.*, "Reconfigurable intelligent surface for interference alignment in MIMO device-to-device networks," in *Proc. IEEE International Conference on Communications Workshops (ICC Workshops)*. IEEE, 2021, pp. 1–6.
- [9] L. Yang *et al.*, "Coverage, probability of SNR gain, and DOR analysis of RIS-aided communication systems," *IEEE Trans. Wireless Commun.*, vol. 9, no. 8, pp. 1268–1272, Aug. 2020.
- [10] M. Di Renzo *et al.*, "Communication models for reconfigurable intelligent surfaces: From surface electromagnetics to wireless networks optimization," *Proc. IEEE*, vol. 110, no. 9, pp. 1164–1209, Sep. 2022.
- [11] S. Abeywickrama *et al.*, "Intelligent reflecting surface: Practical phase shift model and beamforming optimization," *IEEE Trans. Wireless Commun.*, vol. 68, no. 9, pp. 5849–5863, Sep. 2020.
- [12] G. Gradoni and M. Di Renzo, "End-to-end mutual coupling aware communication model for reconfigurable intelligent surfaces: An electromagnetic-compliant approach based on mutual impedances," *IEEE Wireless Commun. Lett.*, vol. 10, no. 5, pp. 938–942, May 2021.
- [13] X. Qian and M. Di Renzo, "Mutual coupling and unit cell aware optimization for reconfigurable intelligent surfaces," *IEEE Wireless Commun. Lett.*, vol. 10, no. 6, pp. 1183–1187, Jun. 2021.
- [14] A. Abrardo *et al.*, "MIMO interference channels assisted by reconfigurable intelligent surfaces: Mutual coupling aware sum-rate optimization based on a mutual impedance channel model," *IEEE Wireless Commun. Lett.*, vol. 10, no. 12, pp. 2624–2628, Oct. 2021.
- [15] D. Badheka *et al.*, "IRS aided communication model for compact MIMO systems," in *Proc. International Conference on Communications*. IEEE, 2021, pp. 1–7.
- [16] S. Shen *et al.*, "Modeling and architecture design of reconfigurable intelligent surfaces using scattering parameter network analysis," *IEEE Trans. Wireless Commun.*, vol. 21, no. 2, pp. 1229–1243, Feb. 2021.
- [17] A. Beck and M. Teboulle, "A fast iterative shrinkage-thresholding algorithm for linear inverse problems," *SIAM journal on imaging sciences*, vol. 2, no. 1, pp. 183–202, 2009.
- [18] P. Mursia *et al.*, "Modeling and optimization of reconfigurable intelligent surfaces in propagation environments with scattering objects," *arXiv preprint arXiv:2302.01739*, 2023.